First Time-Resolved Characterization of Fusion Neutron Spectra via a Liquid Scintillation Detection System in the HL-3 Tokamak*

Jie Zhang,[1,†] Xiu-Lian Chen,[2] Hui-Yin Shen,[2,3] Jing-Long Zhang,[3] Yun-Sheng Zhang,[1] Yu-Xiao Han,[1,4] Qiu-Lei Yang,[1] Yi-Po Zhang,[1,‡] Zhong-bing Shi,[1] and Wei Chen[1]

[1]*Southwestern Institute of Physics, PO Box 432, Chengdu 610041, China*
[2]*College of Physics, Sichuan University, Chengdu 610065, China*
[3]*College of Nuclear Technology and Automation Engineering, Chengdu University of Technology, Chengdu 610059, China*
[4]*University of Science and Technology of China, Hefei, China*

We present, for the first time, our recent advancements in time-resolved fusion neutron spectra measurements and analyses within the HL-3 tokamak. The measurements are executed using a liquid scintillation detector, which has the capacity to discriminate neutrons and γ-rays. Notably, the liquid scintillation detector directly acquires the pulse height spectra of recoil protons in the liquid scintillator, rather than the neutron spectra themselves. To convert the pulse height spectra of recoil protons into neutron spectra, Geant4 simulations are performed to compute the detector response matrix. Subsequently, the GRAVEL method is employed in the neutron spectrum unfolding process. As a result, the time-resolved neutron energy spectra can be obtained through time-resolved pulse amplitude spectra measurements. In this study, the optimal time-resolution for the neutron spectra is 100 ms. This indicates that the HL-3 tokamak is equipped with the ability to conduct research on the temporal evolution of neutron spectra and fast ion velocity distributions.

Keywords: Velocity distribution for fast ions, Neutron spectrum unfolding, Liquid scintillation detector, the GRAVEL method, the HL-3 tokamak

I. INTRODUCTION

One of the fundamental prerequisites for attaining a self-sustained D-T burning plasma is to confine the energetic ions within the fusion plasma for a sufficiently long period to heat the fuel ions [1]. Among the fast fusion ions present in a D-T burning plasma, the fusion-born α particles are of special significance. This is because they play a crucial and indispensable role in fusion ignition. In addition, in D-D fusion plasmas, fast ions generated through auxiliary heating are also of great importance. They enable us to conduct in-depth studies on fast particle interactions [2]. Hence, achieving outstanding confinement quality for fast ions is an inevitable and essential requirement for future fusion reactors. Considerable research efforts have revealed that fast ions are subject to redistribution or expulsion by magnetohydrodynamic (MHD) modes [3–5]. Additionally, experimental observations and theoretical analyses [6] have demonstrated that these ions, in turn, can exert a non-negligible impact on the stability characteristics of MHD modes. Therefore, investigating the behavior of fast ions and their interaction with MHD modes in existing fusion devices holds substantial significance. Within these research efforts, the temporal evolution of fast ion velocity distribution functions represents a crucial parameter.

An important method for diagnosing fast ions in fusion plasmas is by analyzing the neutrons produced in fusion reactions [7]. The energies of these neutrons depend on both the energy released during the reactions and the velocities of the fast-reacting ions. Neutron emission spectrometers (NESs), which measure neutron energy spectra, are thereby sensitive to the velocity distribution functions of these ions. To study the temporal evolution of the fast ion velocity distribution function, it is highly necessary to develop an NES with a sufficiently high time resolution (e.g., on the order of 100 ms). Worldwide, the NESs used for fusion neutron energy spectrum diagnosis mainly include neutron time-of-flight spectrometers [8–10], diamond neutron spectrometers [11, 12], and scintillation neutron spectrometers [13–15]. Among them, neutron time-of-flight spectrometers and diamond neutron spectrometers possess a sufficiently high energy resolution in neutron energy spectrum measurements, yet their time resolution is relatively low (usually $\geq$ 10 s). Although the energy resolution of the scintillation neutron spectrometer in neutron energy spectrum measurements is inferior to that of the neutron time-of-flight spectrometer and the diamond neutron spectrometer, it can achieve neutron energy spectrum measurements with a sufficiently high time resolution. Therefore, the HL-3 tokamak [16] has recently developed a liquid scintillation neutron spectrometer [17], which is mainly used for measuring the temporal evolution of the neutron energy spectrum.

This paper aims to be the first to achieve time resolved neutron spectrum measurement in the HL-3 tokamak by using a liquid scintillation detector in combination with an accurate neutron spectrum-unfolding method. This will provide a powerful diagnostic tool for the research on the fast-ion confinement behavior. This paper is structured as follows: Initially, a liquid scintillation detector is employed to directly measure the pulse amplitude spectrum of recoil protons with a

---

* Supported by the National Magnetic Confinement Nuclear Fusion Energy Development Project of China (Grant No. 2019YFE03020002), the National Natural Science Foundation of China (Grant Nos. 12205085 and 12125502), the Key Research and Development Program of Jiangxi Provincial Fund (Grant No. 20223BBH80006) and the Leading Innovation Research Project of CNNC (Grant No. CNNC-JCYJ-202237) .
† Corresponding author, zhangjie@swip.ac.cn
‡ Corresponding author, zhangyp@swip.ac.cn

specific time resolution (detailed in Section II). Subsequently, an accurate spectrum-unfolding method is utilized to transform the pulse amplitude spectrum of recoil protons into the incident neutron energy spectrum (as presented in Section III). Through these steps, the measurement and analysis of the time evolution of the neutron energy spectrum are successfully carried out (covered in Section IV). Finally, a comprehensive summary of this paper is provided in Section V.

II. EXPERIMENTAL MEASUREMENTS

In this section, a detailed introduction is provided regarding the experimental setup, the properties of the liquid scintillation neutron spectrometer, as well as the experimental determination of the pulse amplitude spectrum.

A. Experimental setup

The liquid scintillation neutron spectrometer is positioned on the east side of the HL-3 tokamak. It is employed to measure the neutron spectrum during neutral beam injection (NBI). The experimental layout is depicted in Fig. 1. In the figure, 'NBI' denotes the neutral beam injection system, while 'LSD' represents the liquid scintillation detector.

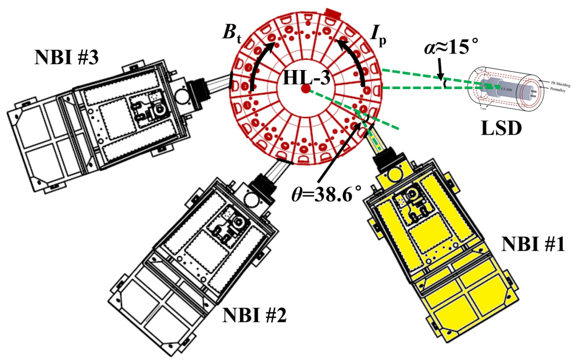

Fig. 1. (Color online) The layout of experimental devices (NOT TO SCALE).

The design parameters of HL-3 are presented as follows [16]: the plasma current I_p ranges from 2.5 to 3 MA, the toroidal field B_t varies between 2.2 and 3 T, the major radius R is 1.78 m, the minor radius a is 0.65 m, the elongation κ is less than or equal to 1.8, and the triangularity δ is less than or equal to 0.5. The research program of HL-3 centers on the crucial issues in the development of advanced divertor concepts and high-heat-flux components. Moreover, it also focuses on high-performance operation scenarios to support ITER and the subsequent fusion reactors, as stated in references [18, 19].

The HL-3 tokamak is planned to be equipped with three NBI beamlines. Among them, the No.1 and No.2 NBI beamlines are in the same direction as the plasma current, while the No.3 NBI beamline is in the opposite direction to the plasma current. During the occurrence of this experiment in 2024, only the No.1 NBI beamline [20] was in operation, and its injection angle was 38.6°.

The liquid scintillation neutron spectrometer employs an EJ-309 liquid scintillation detector, which is paired with a 500-Msps, 12-bit digitizer [17]. The measured neutron and γ/X-ray spectra are directly processed through programming on a Field Programmable Gate Array (FPGA). In an attempt to elevate the neutron count rate and, in turn, improve the time resolution of the neutron spectrum, the EJ-309 liquid scintillation detector is shielded against both γ/X-rays and magnetic fields. A 3-cm-thick Pb layer is used for γ/X-ray shielding, and a 3-mm-thick permalloy layer is applied for magnetic shielding. Notably, it is deliberately left without any shielding components or collimators specifically designed for neutrons, ensuring that neutrons can reach the detector unimpeded and be detected with high efficiency. The detector is approximately 8 m away from the central axis of the HL-3 tokamak and has an angular separation of about 15° with respect to its radial direction.

B. Verification of n/γ discrimination

A high-performance thermonuclear plasma serves as a powerful source of nuclear radiation. This radiation encompasses neutron emission resulting from the main fusion reactions and γ-rays generated by the interaction of supra-thermal ions with plasma impurities [21]. In fact, aside from neutron emissions and γ-rays, the radiation field of a nuclear fusion device also contains a large amount of hard X-rays. These hard X-rays originate from the interaction between the runaway electron beam and the wall materials. During neutral beam injection, not only is the measurement of the γ/X-ray spectrum affected by neutron radiation [22], but the measurement of neutrons is also influenced by γ/X-rays [23].

Previous experimental results have indicated that the EJ-309 liquid scintillation detector demonstrates excellent n/γ discrimination capabilities [17]. However, with the increase in NBI power, the neutron yield will increase accordingly. As a result, both the neutron count rate and the γ/X count rate of the detector will increase significantly, and under such circumstances, the n/γ discrimination ability will decline. Since this paper focuses on measuring the time-evolution of the fusion neutron spectrum, it is necessary for us to confirm the n/γ discrimination ability under conditions of high neutron yield. The confirmation method is to compare it with the neutron flux monitor (NFM) based on the fission chamber detector [24]. The reason for choosing the fission chamber detector as a reference is that it has almost no response to γ/X-rays, and its signal can be considered as a purely neutron signal. The experimental measurement data are presented in Fig. 2.

In Fig. 2, two adjacent discharges, namely shot #6002 and shot #6003, are selected. These two shots have similar plasma currents (about 300 kA) and the maximum NBI power (1.3 - 1.4 MW). The difference between them lies in the different durations of NBI. In shot #6002, the NBI lasts from 1100 ms to 1600 ms, with a duration of 500 ms, while

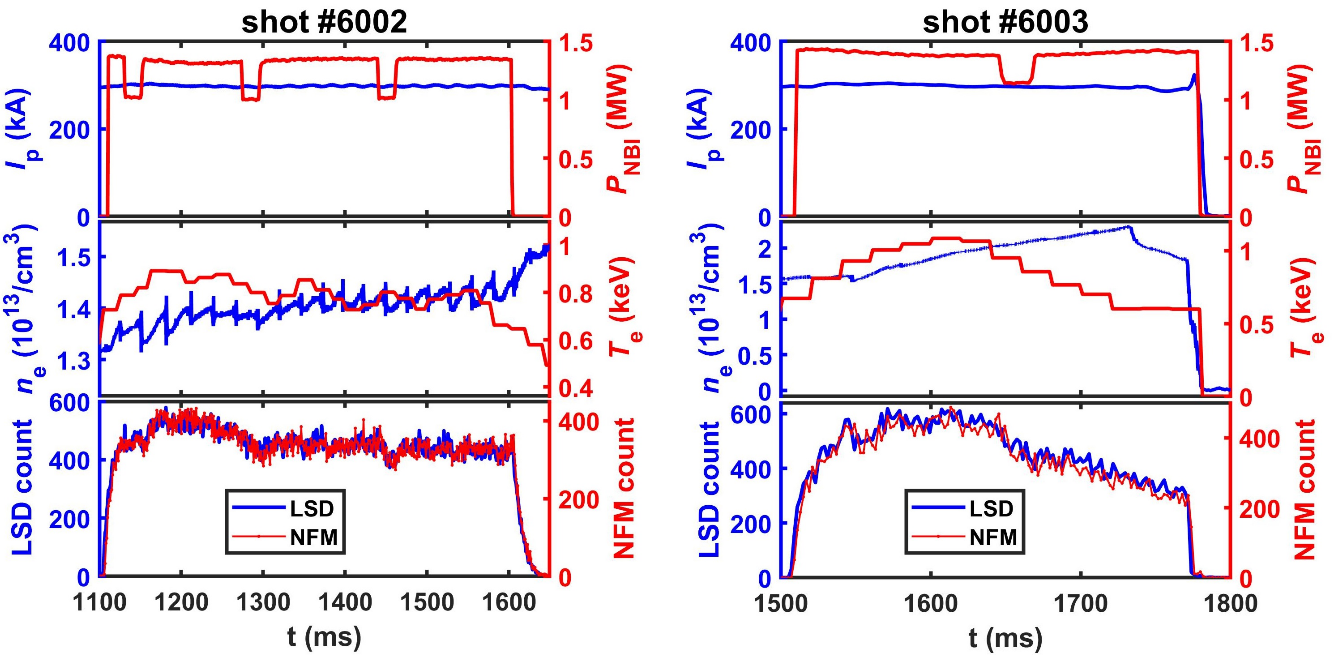

Fig. 2. (Color online) Time traces of some key parameters for shot #6002 (left panel) and shot #6003 (right panel). The parameters include: 'I_p' (plasma current), 'P_NBI' (NBI power), 'n_e' (line-averaged electron density), 'T_e' (electron temperature), 'LSD count' (the count of the liquid scintillation detector), and 'NFM count' (the count of the neutron flux monitor).

in shot #6003, the NBI lasts from 1510 ms to 1780 ms, with a duration of 270 ms. The reason is that a plasma disruption occurred at about 1780 ms in shot #6003, which led to an abrupt drop of both the plasma current and the NBI power to 0. In terms of neutron flux measurement, except for the absolute count, the variation trends of the measurement data from the liquid scintillation detector and the fission chamber detector almost completely coincide. Therefore, the experimental data demonstrate that the liquid scintillation detector still exhibits excellent n/γ discrimination performance under the corresponding count rate conditions.

For shot #6002, at the end of the NBI, the neutron flux data still remain at a relatively high level, and then the neutron flux decays exponentially. This process reflects the slowing-down behavior of fast ions in the plasma [25]. Based on the data, the fast-ion confinement time corresponding to the plasma parameters is roughly estimated to be on the order of tens of milliseconds. For shot #6003, at the moment of the disruption, the neutron flux drops abruptly to 0, indicating that after the plasma disruption occurs, there is no time for the fast-ion slowing-down process to take place.

Excellent n/γ discrimination performance indicates that the liquid scintillation neutron spectrometer is capable of identifying neutron signals from a large number of pulses, thereby obtaining the correct pulse amplitude spectrum of neutron signals. The PSD parameter is defined as the pulse-shape discrimination factor, which can be expressed by the following formula.

$$PSD = 1 - \frac{Q_{slow}}{Q_{total}} \quad (1)$$

in which, Q_{slow} and Q_{total} represent the charge in the slow components and the total charge of the current pulse [26], respectively. The n/γ discrimination effect of the liquid scintillation neutron spectrometer is shown in Fig. 3.

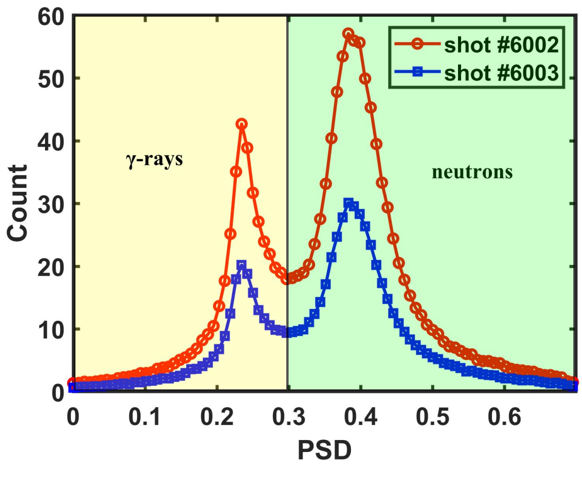

Fig. 3. (Color online) The n/γ discrimination effect of the liquid scintillation neutron spectrometer. The light-yellow area represents the γ/X-ray signals, while the light-green area represents the neutron signals.

As can be seen from Fig. 3, although the neutron signals and γ/X-ray signals overlap near the PSD value of 0.3, both types of signals can form distinct peaks. This indicates that the liquid scintillation neutron spectrometer indeed has an ex-

cellent ability to distinguish between neutrons and γ/X-rays. In the figure, the height of the γ/X-ray peak is lower and the width is narrower than that of the neutron peak, suggesting that more neutron signals are measured by the liquid scintillation neutron spectrometer. This is due to the presence of a γ/X-ray shield around the liquid scintillation neutron detector while there is no neutron shield at all.

In fact, the overlapping part is mainly caused by the superposition of low-amplitude pulse signals under high-count-rate conditions. There are mainly two reasons: First, the pulse amplitude spectrum measured in the experiment is a continuous spectrum, and the number of low-amplitude pulse signals is much larger than that of high-amplitude pulse signals. Therefore, it is mainly the low-amplitude pulses that are superimposed. Second, even if a low-amplitude pulse is superimposed with a high-amplitude pulse, the low-amplitude pulse is not likely to affect the discrimination result of the high-amplitude pulse. Compared with low-amplitude pulse signals, high-amplitude pulse signals are the key research objects in neutron spectrum measurements. Therefore, the overlapping part has a very limited impact on the measurement of fusion neutron spectra.

C. Pulse amplitude spectrum measurements

Having verified the n/γ discrimination performance of the liquid scintillation neutron spectrometer, we can derive the so-called neutron pulse amplitude spectrum by conducting a statistical analysis of the amplitude distribution of neutron pulses. In Fig. 2, the time resolution of the neutron count evolution curve is 1 ms. Nevertheless, it is quite clear that the time resolution achievable in neutron pulse amplitude spectrum measurement cannot reach 1 ms. The reason lies in the fact that a few hundred counts simply cannot constitute a pulse amplitude spectrum with statistical significance. Empirically, to ensure that the measured pulse amplitude spectrum has statistical significance, the total count across the full spectrum must reach the order of 10^4. By making an estimate based on the data presented in Fig. 2, we find that the neutron count rate is roughly on the order of several hundred kcps. As a result, the time resolution of the neutron pulse amplitude spectrum measurement is on the order of 100 ms.

Indeed, the measurement of the neutron pulse amplitude spectrum with this time resolution is fully capable of fulfilling the prerequisites for the investigation into the evolution of the fast ion velocity distribution within the HL-3 tokamak. As previously declared in the introduction, these requirements have been precisely defined to guide the relevant research. Under this background, we measured the neutron pulse amplitude spectra of shot #6002 and shot #6003 with a time resolution on the order of 100 ms, as depicted in Fig. 4.

As depicted in Fig. 4, the neutron pulse amplitude spectrum in Fig. 4(a) has a time resolution of 300 ms, whereas the one in Fig. 4(b) features a time resolution of 100 ms. Both spectra demonstrate good statistical properties. Evidently, Fig. 4 shows that we have successfully accomplished the measurement of the neutron pulse amplitude spectrum with a time resolution of 100 ms.

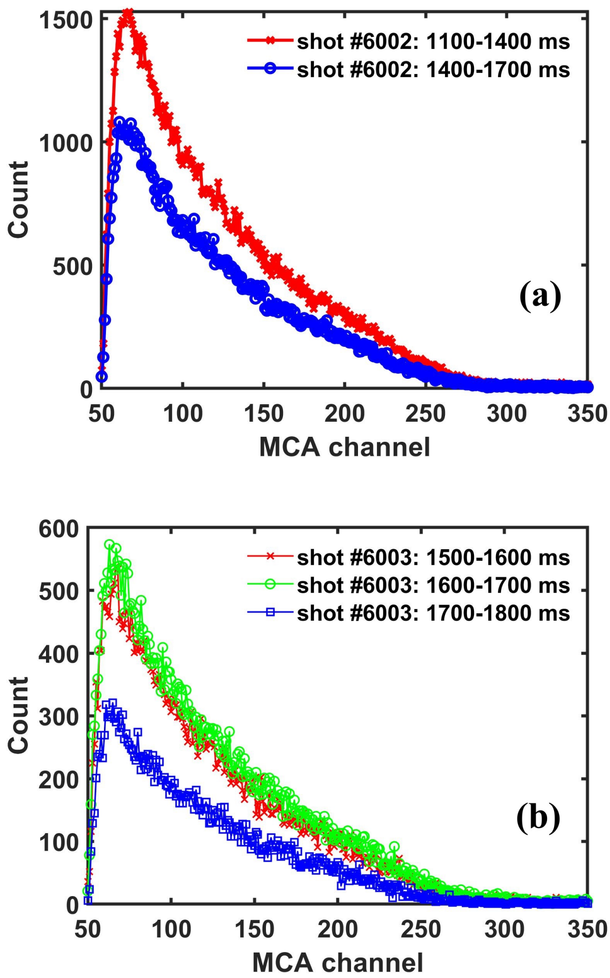

Fig. 4. (Color online) The measured neutron pulse amplitude spectra for (a) shot #6002 and (b) shot #6003.

Nevertheless, simply measuring the evolution of the pulse amplitude spectrum is insufficient for analyzing the evolution behavior of the fast ion velocity distribution. The reason lies in the fact that the various neutron pulse amplitude spectra presented in the figure share similar shapes. This similarity poses a significant challenge in detecting subtle differences among them. Additionally, it is extremely difficult, if not impossible, to clarify the corresponding relationship between the pulse amplitude spectrum and the fast ion velocity distribution.

In order to fulfill the purpose of this study, that is, to acquire the measurement of fusion neutron spectra with a time resolution of 100 ms, it is essential to carry out in-depth research on the neutron spectrum unfolding, whose ultimate goal is to enable the conversion from neutron pulse amplitude spectra to neutron spectra. In this paper, 'neutron spectrum' refers to the 'energy spectrum of neutrons'.

III. NEUTRON SPECTRUM UNFOLDING

In this section, the GRAVEL method is adopted to conduct neutron spectrum unfolding. This process encompasses several crucial aspects: the energy calibration of the liquid scintillation neutron spectrometer, which is fundamental for accurate energy determination; the meticulous calculation of the detector response matrix for neutrons, enabling a proper understanding of how the detector responds to neutrons of different energies; and iterative spectrum unfolding, a step-by-step refinement process to obtain the most accurate neutron spectrum. This systematic approach ensures the precision and reliability of the neutron spectrum unfolding.

A. the GRAVEL method

The GRAVEL method represents an iterative unfolding algorithm that makes a minor modification to the SAND-II algorithm. The iterative process of the GRAVEL method for deriving the neutron spectrum is illustrated by the following equations [27, 28].

$$\phi_j^{k+1} = \phi_j^k \exp\left[\frac{\sum_i W_{ij}^k \ln\left(\frac{N_i}{\sum_{j'} R_{ij'}\phi_{j'}^k}\right)}{\sum_i W_{ij}^k}\right] \tag{2}$$

in which, N_i denotes the measured count of the ith channel in the neutron pulse amplitude spectrum, where i is the channel address index. ϕ_j^k represents the neutron count in the jth energy interval of the neutron energy spectrum after kth iteration, with j and j' being the energy interval indices. k stands for the iteration number. R_{ij} is the response matrix coupling the ith pulse height interval to the jth energy interval, and W_{ij}^k is a weight factor defined as,

$$W_{ij}^k = \frac{R_{ij}\phi_j^k N_i}{\sum_{j'} R_{ij'}\phi_{j'}^k} \tag{3}$$

For the iterative algorithm adopted in this paper, the stopping conditions are set as follows. The iterative index J^k needs to be made small enough (for instance, less than 0.1 or 0.01; the actual value is related to the experimental data). Meanwhile, the number of iterations k is required to be no more than 300, since a large k can easily result in overfitting. The iterative index J^k is expressed by the equation below [29].

$$J^k = \frac{\sum_i \left(N_i - R_{ij} * \phi^k\right)^2}{\sum_i R_{ij} * \phi^k} \tag{4}$$

in which, ϕ^k denotes the full neutron energy spectrum after kth iteration.

It is quite apparent that, based on Equations. (2) to (4), provided that the response matrix and the pulse amplitude spectrum are known, the neutron energy spectrum ϕ can be retrieved via spectrum unfolding. Nevertheless, up to the present moment, only the pulse amplitude spectrum has been experimentally determined. Consequently, the acquisition of the response matrix stands as an essential condition for the successful unfolding of the neutron energy spectrum.

B. Energy calibration

The response matrix of a liquid scintillation detector to neutrons can generally be obtained through calculation. However, prior to calculating the response matrix, energy calibration of the detector is essential. Unlike the energy calibration of commonly used gamma detectors, that of liquid scintillation detectors is more intricate. This is primarily because neither full - energy peaks are detectable when measuring neutrons and γ/X-rays with a liquid scintillation detector. Given the impracticality of obtaining an absolutely mono-energetic neutron beam, this paper employs ^{137}Cs and ^{60}Co gamma sources for the energy calibration of the liquid scintillation detector. Although full energy peaks still do not appear in the measured gamma pulse amplitude spectrum, the Compton edges can assist us in determining the correspondence between energy and the channel addresses of the multi-channel analyzer (MCA), thereby achieving energy calibration, as illustrated in Fig. 5.

In Fig. 5(a), the Compton edge of the 0.662 MeV gamma rays emitted by the ^{137}Cs gamma source can be observed. In Fig. 5(b), two Compton edges are visible. From the low - energy to the high - energy side, these Compton edges correspond to the 1.171 MeV and 1.332 MeV gamma rays emitted by the ^{60}Co gamma source, respectively. The Compton edge corresponds to the maximum energy of recoil electrons generated by Compton scattering, and its energy can be expressed by the following equation [30].

$$E_c = \frac{2E_\gamma^2}{m_e c^2 + 2E_\gamma} \tag{5}$$

in which, E_c denotes the energy corresponding to the Compton edge, E_γ represents the initial energy of the gamma rays emitted by the radioactive source, m_e stands for the rest mass of the electron, c signifies the speed of light.

After determining the energy corresponding to the Compton edge, it is also necessary to determine the MCA channel corresponding to the Compton edge. According to previous studies [31], the MCA channel corresponding to the Compton edge can be expressed by the following equation.

$$n_c = \bar{n} + 1.177\sigma \tag{6}$$

in which, n_c denotes the MCA channel corresponding to the Compton edge. If the Compton edge is fitted using a Gaussian function, the expected value $\bar{n}$ and the standard deviation σ can be obtained (see Fig. 5).

Based on Equations. (5) and (6), the energy and the corresponding MCA channel of the Compton edge can be obtained. Subsequently, an energy calibration curve can be plotted (as shown in Fig. 6), thereby accomplishing the energy

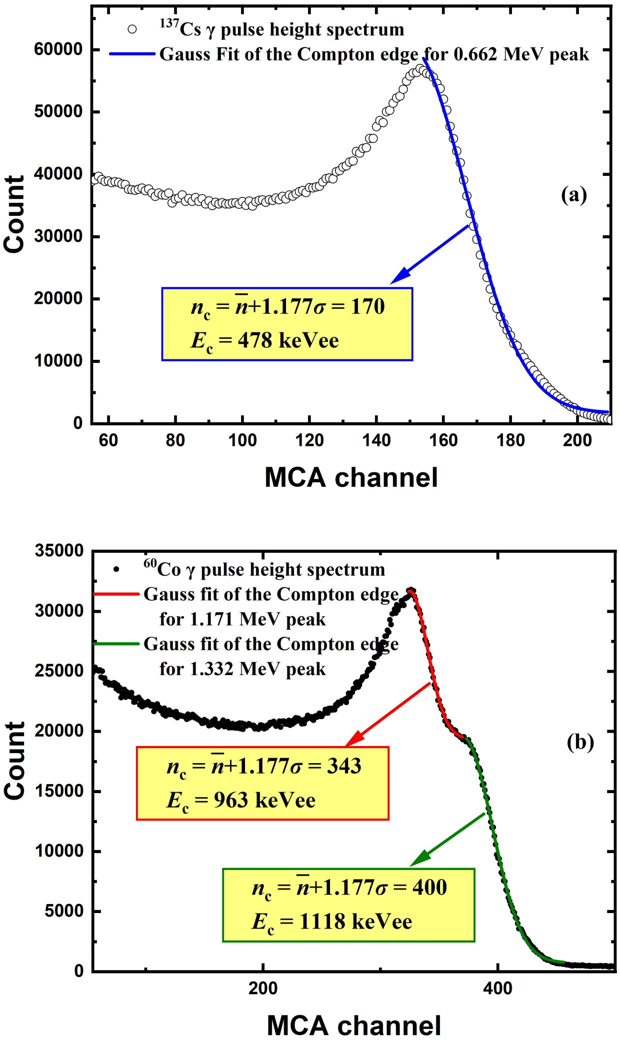

Fig. 5. (Color online) The measured gamma pulse amplitude spectra for (a) ^{137}Cs and (b) ^{60}Co gamma sources. The Compton edges can help to determine the correspondence between energy and MCA channel.

calibration of the liquid scintillation detector. As can be observed from the figure, there is an excellent linear relationship between the energy and the MCA channel. It should be noted that the ordinate in the figure represents the light output, measured in electron equivalent energy (keVee), which essentially refers to the electron deposited energy.

C. Response matrix calculations

The response function of a detector is defined as the differential pulse height distribution for incident mono-energetic radiations and is determined by the cross-sections of photon interactions within the detector [32].This initial response function is broadened by multiple factors. There are variations in light generation and light collection efficiency. Photon production in a scintillator has a statistical nature, the number of generated electrons in the detector fluctuates, the detector has inherent variations, and there is electronic noise. Together, these elements - light generation variation, statistical photon production, light collection efficiency variation, electron generation fluctuation, detector inherent variation, and electronic noise - broaden the initial response function [33].

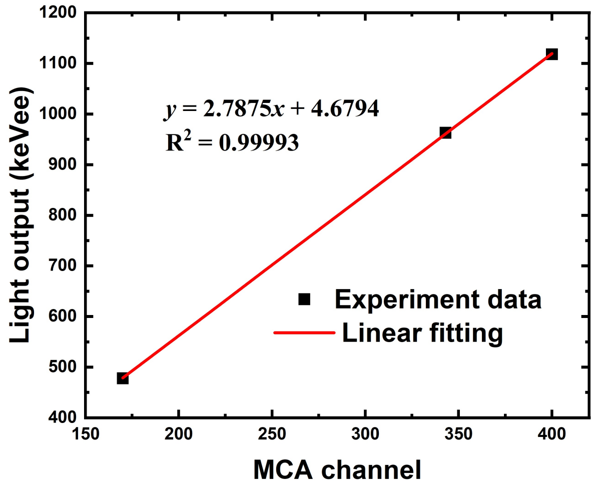

Fig. 6. (Color online) The energy calibration curve.

To accurately describe the response function in relation to the measured spectra, individual and collective calculations of the physical effects that each factor has on broadening are necessary. However, this process is highly intricate. Instead of computing each physical phenomenon separately, the Gaussian Energy Broadening (GEB) treatment in MCNP offers a virtual peak broadening mechanism [34]. This mechanism encompasses all the broadening effects, simplifying the complex calculation process. The peaks of the initial spectrum must be broadened into Gaussian peak shapes with distinct full widths at half maximum (FWHM) based on their respective energies. The FWHM can be expressed by the following equation.

$$\mathrm{FWHM} = a + b\sqrt{E + cE^2} \tag{7}$$

in which, E represents the energy, with the unit of keVee. The GEB coefficients a, b, and c are fitting parameters, the values of which need to be determined through experiments.

Since the full-energy peak of gamma rays cannot be measured using a liquid scintillation detector, and the peak corresponding to the measured Compton edge does not follow a Gaussian distribution, the GEB parameters cannot be fitted by obtaining the FWHM. In this paper, an alternative method is adopted to obtain the GEB parameters. First, the gamma energy spectra of ^{137}Cs and ^{60}Co before broadening are calculated based on the Geant4 code [35]. Then, the GEB parameters are scanned within a certain range. For each set of GEB parameters, the broadened gamma energy spectrum is calculated, and the standard deviation between the calculated spectrum and the normalized experimental spectrum is deter-

mined. Finally, the set of GEB parameters that yields the minimum standard deviation between the calculated and experimental spectra is selected. The method determines the GEB parameters as follows: $a = 21.6$, $b = 0.114$, $c = 0.36$. Fig. 7 presents the comparison diagrams between the experimental γ-ray spectra of ^{137}Cs and ^{60}Co and the corresponding γ-ray spectra simulated by Geant4.

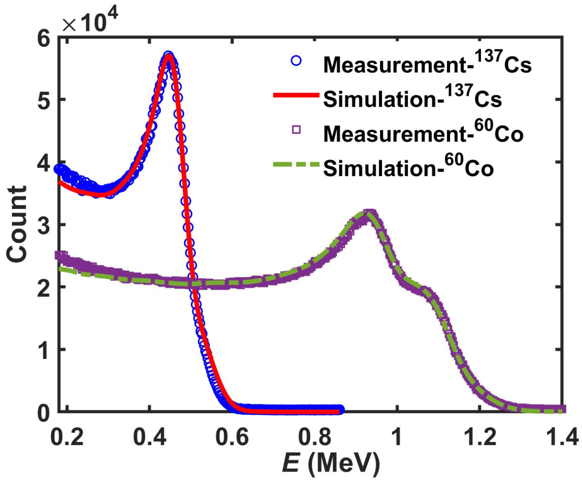

Fig. 7. (Color online) Comparison diagrams of the experimental γ-ray spectra of ^{137}Cs and ^{60}Co with the γ-ray spectra simulated by Geant4.

As can be observed from Fig. 7, apart from a slight deviation between the Geant4 simulated γ-ray spectrum and the experimental γ-ray spectrum at the low energy part, the two spectra exhibit a high degree of overall agreement. This indicates that the Geant4 simulated γ-ray spectrum broadened using the GEB parameters provided in this paper can accurately represent the response function of the liquid scintillation detector to γ-rays. At the low energy part of the γ-ray spectrum, the deviation between the Geant4 simulated γ-ray spectrum and the experimental γ-ray spectrum is presumably due to the fact that electronic noise and background γ radiation were not taken into account in the simulation.

Although the calculation of the response function of the liquid scintillation detector to γ-rays has been achieved, the response of the liquid scintillation detector to neutrons is not entirely the same as that to γ-rays. Therefore, it is necessary for us to conduct research on the detector's response to neutrons. The main difference between the responses of the liquid scintillation detector to neutrons and γ-rays lies in the fact that neutrons generate fluorescence in the scintillator through recoil protons, while γ-rays emit fluorescence via recoil electrons. Moreover, recoil protons and recoil electrons of the same energy induce different light outputs. The semi-empirical formula for calculating the light output of recoil protons in the scintillator is presented as follows [36].

$$L(E_\mathrm{p}) = AE_\mathrm{p} - B\left(1 - e^{-CE_\mathrm{p}^D}\right) \tag{8}$$

where the light output $L(E_\mathrm{p})$ is expressed in electron equivalent units. E_p represents the proton energy, and A, B, C, and D are the fitted parameters. For the 2-inch EJ-309 liquid scintillation detector, $A = 0.62$, $B = 1.3$, $C = 0.39$, $D = 0.97$ [36].

After incorporating Equation. (8) into the Geant4 simulation, it becomes possible to calculate the response function of the liquid scintillator to neutrons. To verify the accuracy of the response function calculations, we measured the energy spectrum of the Am-Be neutron source in Sichuan University [37] using the liquid scintillation detector. Subsequently, we carried out calculations with Geant4 code based on the experimental conditions, thereby obtaining the simulated energy spectrum of the Am-Be neutron source. The comparison between the experimental and simulated spectra is presented in Fig. 8.

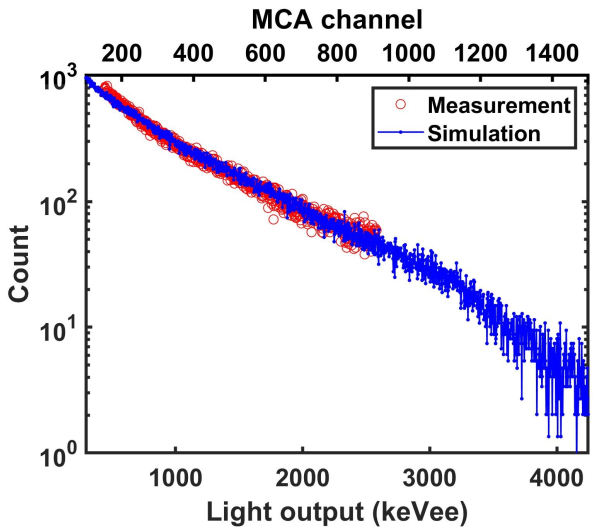

Fig. 8. (Color online) Comparison diagrams of the experimental neutron spectrum of the Am-Be neutron source with the neutron spectrum simulated by Geant4.

As shown in Fig. 8, there is a good agreement between the experimental neutron spectrum and the simulated neutron spectrum. The experimental data are only capable of measuring the energy range presented in the figure. This result validates the feasibility of using Geant4 code to accurately calculate the response matrix of the liquid scintillation detector to neutrons.

To obtain the response matrix of the liquid scintillation neutron spectrometer for fusion neutrons on the HL-3 tokamak, a simplified model was developed using Geant4 for the application scenario of this spectrometer. Since the liquid scintillation neutron spectrometer developed for HL-3 is primarily used to measure the energy spectrum of D-D fusion neutrons (about 2.45 MeV), in principle, it is only necessary to cover neutrons within the energy range of 2 - 3 MeV. The neutron emission profile is regarded as an elliptical profile, and Gaussian distribution sampling is required in both the radial and vertical directions [38]. The geometric dimensions considered in the Geant4 simulation are similar to those of HL-3, but the model only includes a simplified vacuum vessel and the first wall. The response matrix of the liquid scintilla-

tion neutron spectrometer to neutrons calculated by Geant4 is shown in Fig. 9.

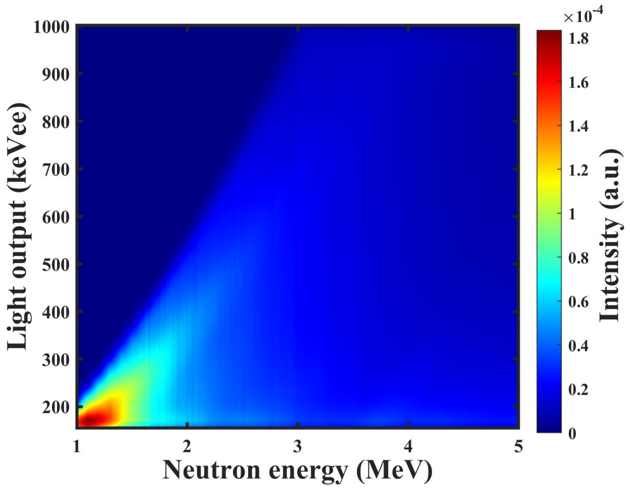

Fig. 9. (Color online) The response matrix of the liquid scintillation neutron spectrometer to neutrons calculated by Geant4.

D. Spectrum unfolding and verification

Currently, the response matrix and the neutron pulse amplitude spectrum have been obtained, so the spectrum can be unfolded using the GRAVEL method described in section III A.

To verify the correctness of the spectrum unfolding method, we define three cases of D-D neutron spectra here.

Case 1: The peak energy $\mu_1 = 2.3$ MeV and the ion temperature $T_{\mathrm{i}1} = 4$ keV.

Case 2: The peak energy $\mu_2 = 2.45$ MeV and the ion temperature $T_{\mathrm{i}2} = 2$ keV.

Case 3: The peak energy $\mu_3 = 2.6$ MeV and the ion temperature $T_{\mathrm{i}3} = 1$ keV.

In a plasma, the Doppler shift phenomenon may occur in the neutron energy spectrum, and this phenomenon has been observed in magnetically confined fusion devices [39]. Therefore, setting different peak energies here is to consider whether the Doppler - shifted neutron energy spectra can be unfolded correctly. Different ion temperatures in the plasma will lead to different broadenings of the neutron energy spectrum. Different ion temperatures are set to verify whether neutron energy spectra with different broadenings can be correctly unfolded.

In a thermonuclear fusion plasma in thermal equilibrium, the ion velocities follow a Maxwellian distribution, and the neutron energy spectrum generated by the fusion of fuel ions follows a Gaussian distribution, and its FWHM in keV is shown in the following equations [40].

$$\begin{aligned} \mathrm{FWHM_{DD}} &= 82.54\sqrt{T_{\mathrm{i}}(\mathrm{keV})} \\ \mathrm{FWHM_{DT}} &= 177.3\sqrt{T_{\mathrm{i}}(\mathrm{keV})} \end{aligned} \tag{9}$$

where $\mathrm{FWHM_{DD}}$ refers to the full width at half maximum of the D-D fusion neutron energy spectrum, $\mathrm{FWHM_{DT}}$ refers to the full width at half maximum of the D-T fusion neutron energy spectrum, and $T_{\mathrm{i}}(\mathrm{keV})$ represents the ion temperature with the unit of keV.

According to Equation. (9), the FWHM of the D-D neutron energy spectrum for each case can be obtained. For case 1, the FWHM of its neutron energy spectrum is 165 keV. For case 2, the FWHM of its neutron energy spectrum is 117 keV. For case 3, the FWHM of its neutron energy spectrum is 85 keV.

In the Geant4 simulation, initial neutron energy spectra with Gaussian distributions are respectively set for the above three cases. Then, the response functions of the liquid scintillation neutron spectrometer to neutrons under the three cases are calculated separately, which are the simulated neutron pulse amplitude spectra. Combining with the response matrix (as shown in Fig. 9), the GRAVEL method can be used to unfold the neutron energy spectrum. The unfolding neutron energy spectra are compared with the initially set simulation neutron energy spectra in the three cases, and the results are presented in Fig. 10.

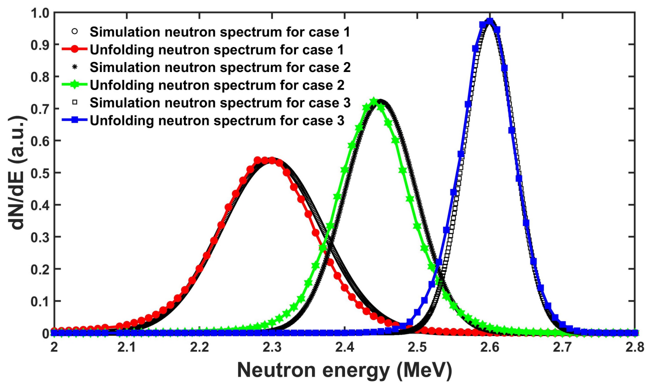

Fig. 10. (Color online) Comparisons between unfolding neutron energy spectra and simulation neutron energy spectra.

Fig. 10 illustrates three neutron peaks conforming to Gaussian distributions. In the order from left to right, they respectively correspond to case 1, case 2, and case 3. Each of these neutron peaks demonstrates unique peak energies and peak widths. Notably, for each individual neutron peak, a remarkable agreement can be observed between the simulation neutron spectrum and the spectrum retrieved via the unfolding procedure.

To further evaluate the performance of the spectrum unfolding, we conducted a comparison between the simulation pulse amplitude spectra and the unfolding pulse amplitude spectra for the three cases. The results are presented in Fig. 11.

It can be clearly observed from Fig. 11 that the pulse amplitude spectra under the three cases have distinct maximum MCA channels. This indicates that the neutron energy spectra in the three cases possess different energy levels. Specifically, the maximum energy of case 1 is the lowest among the three, followed by that of case 2, and the maximum energy of case 3 is the highest, which is in accordance with the peak energies of the three cases. Moreover, it is visually evident that the unfolding pulse amplitude spectra are in good overall agreement

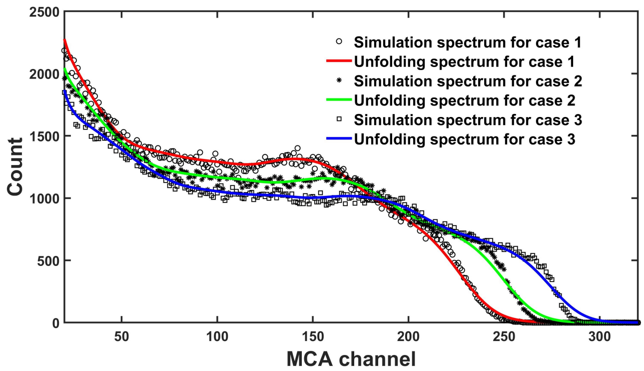

Fig. 11. (Color online) Comparisons between unfolding neutron pulse amplitude spectra and simulation neutron pulse amplitude spectra.

with the simulation pulse amplitude spectra.

IV. EXPERIMENTAL DATA ANALYSES

Since Fig. 10 and 11 have validated the correctness of the spectrum unfolding method from the perspectives of the neutron energy spectrum and the neutron pulse amplitude spectrum respectively, the next step is to apply this spectrum unfolding method to conduct a spectrum unfolding study on the neutron pulse amplitude spectra measured in the experiment shown in section II C. For the very first time, this section is set to reveal the measurement findings of the time-dependent evolution of the neutron energy spectrum obtained from the HL-3 tokamak.

Fig. 12 presents the results of unfolding the neutron pulse amplitude spectra measured by the liquid scintillation neutron spectrometer for shots #6002 and #6003 in the HL-3 tokamak using the GRAVEL method. Moreover, it visually demonstrates the unfolding effect from the perspective of the pulse amplitude spectra. Specifically, Fig. 12(a) depicts the neutron energy spectra obtained by unfolding the neutron pulse amplitude spectra of shot #6002. Fig. 12(b), corresponding to Fig. 12(a), shows the neutron pulse amplitude spectra, which clearly reveal the unfolding effect. Similarly, Fig. 12(c) shows the neutron energy spectra derived from the neutron pulse amplitude spectra of shot #6003. Fig. 12(d), corresponding to Fig. 12(c), presents the neutron pulse amplitude spectra, effectively demonstrating the unfolding outcome. As can be seen from Fig. 12(b) and (d), the spectrum unfolding effects in Fig. 12(a) and (c) are quite good. This is because the pulse amplitude spectra obtained through unfolding are highly consistent with the experimentally measured pulse amplitude spectra. The relatively obvious discrepancies only occur at the low energy end (see the yellow area in the figures). This discrepancy is predominantly attributed to electronic noise, low energy scattered neutrons, and inaccurately identified γ signals.

From the shape of the neutron spectrum in Fig. 12(a), the neutron energy spectra in two different time periods both exhibit a peaked distribution. However, the shape of the spectra, especially the blue neutron spectrum, deviates from the Gaussian distribution. This phenomenon is quite understandable because in the NBI plasma, the ion velocity distribution has already deviated from the Maxwellian distribution. The low energy ends of the two neutron spectra are significantly elevated compared to the high energy ends. The reasons for this result mainly include two aspects: The environment where the detector is located is filled with a large number of scattered neutrons with relatively low energy; Under high count rate conditions, the liquid scintillation neutron spectrometer cannot completely distinguish the low amplitude n/γ pulse signals (see Fig. 3).

In addition, the peak energy of the blue neutron spectrum is approximately 2.35 MeV, which deviates by 0.1 MeV from the typical energy of D-D fusion neutrons, 2.45 MeV. The likely reason for this result is that the anisotropy of the fast ion velocity distribution becomes prominent, leading to a significant increase in the Doppler-shift component. In terms of the measurement time, the measurement time for both neutron spectra is 300 ms, which means that the time resolution of the liquid scintillation neutron spectrometer can reach 300 ms. Moreover, the neutron flux during the time corresponding to the red neutron spectrum in Fig. 12(a) is higher than that during the time corresponding to the blue neutron spectrum (see Fig. 2). And during the time corresponding to the blue neutron spectrum, the anisotropic component of fast ions increases. This phenomenon may indicates that the anisotropy of fast ions is detrimental to the confinement characteristics of fast ions.

As depicted in Fig. 12(c), three neutron energy spectra, each measured within a 100 ms time span, are presented. This vividly demonstrates that the liquid scintillation neutron spectrometer installed on the HL-3 tokamak has successfully accomplished neutron energy spectrum measurements with a remarkable time resolution of 100 ms. In the realm of plasma physics, plasma disruption represents a crucial research frontier. The successful realization of 100 ms time-resolved neutron energy spectrum measurements has opened up new possibilities for the HL-3 tokamak to explore plasma disruption from the vantage point of the evolution of the ion velocity distribution. A close examination of the three spectra in Fig. 12(c) reveals that they bear a strong resemblance in terms of shape. Despite a subtle tendency of the peak energy to shift towards the lower energy range, this trend is rather inconspicuous. This implies that the fast ion velocity distribution within this NBI plasma remains relatively stable without any distinct alterations. Nevertheless, it should be noted that to comprehensively investigate the changes in the fast ion velocity distribution prior to the moment that plasma disruption occurs, a more extensive dataset regarding the evolution of the neutron energy spectrum is indispensable.

According to the measurement results of the charge exchange recombination spectroscopy (CXRS) diagnostics, the core ion temperatures of shots #6002 and #6003 are approximately 1 keV. In a thermally equilibrated plasma, the FWHM of the neutron energy spectrum is approximately 82 keV. The FWHM of the neutron energy spectrum shown in Fig. 12(a)

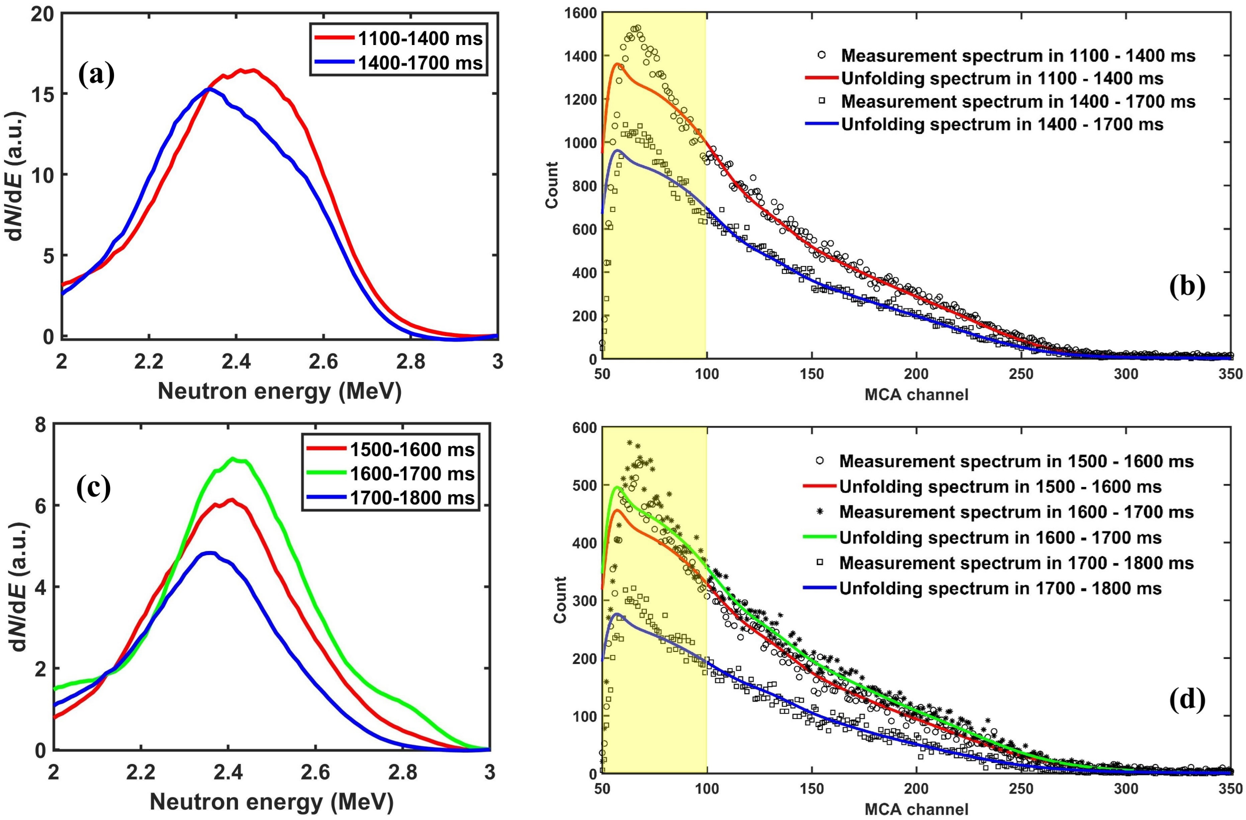

Fig. 12. (Color online) Time evolution of the unfolding neutron spectrum normalized to the same NBI power for (a) shot #6002 and (c) shot #6003,and the actual unfolding effect for (b) shot #6002 and (d) shot #6003 from the perspective of neutron pulse amplitude spectra.

is approximately 0.4 MeV, and that shown in Fig. 12(c) is approximately 0.35 MeV. This FWHM is significantly several times wider than that of the neutron energy spectrum generated by a thermally equilibrated plasma. There are two possible reasons for this result: Firstly, a large number of fast ions exist in the NBI plasma, causing the ion velocity distribution to deviate significantly from the Maxwellian distribution, which leads to a larger width. Secondly, the liquid scintillation neutron spectrometer is not equipped with a neutron collimator, allowing neutrons generated throughout the entire plasma to enter the detector and be counted in the energy spectrum. Since the neutron energy spectra generated at different spatial positions have different degrees of Doppler shift, the width of the neutron spectrum increases significantly. In addition, it can be seen that shot #6002 has a wider neutron energy spectrum than shot #6003. This is due to the differences in the fast ion velocity distributions between the two shots caused by different plasma parameters (see n_{e} and T_{e} in Fig. 2) and MHD activities (see Fig. 13). From Fig. 13(a), it can be observed that the plasma in shot #6002 predominantly exhibits significant sawtooth instability. Fig. 13(b) reveals that the plasma in shot #6003 is characterized by multiple MHD instabilities, among which the 1/1 mode dominates with its frequency gradually increasing over time.

V. SUMMARY

To study the time evolution of the fast ion velocity distribution in the plasma, the HL-3 tokamak has recently developed a neutron spectrometer based on a liquid scintillation detector. The liquid scintillation detector has excellent n/γ discrimination capabilities, enabling it to be used for measuring the neutron pulse height spectrum with a certain time resolution in the fusion neutron field.

First, this paper verified the outstanding n/γ discrimination performance of the liquid scintillation neutron spectrometer by comparing it with the neutron flux measurement system based on a fission chamber in measuring the neutron flux evolution curve. Then, the liquid scintillation neutron spectrometer was used to measure the neutron pulse height spectrum with a certain time resolution (on the order of hundreds of milliseconds) on the HL-3 tokamak. Next, a complete GRAVEL spectrum unfolding method (including the spectrum unfolding algorithm, energy calibration of the liquid scintillation detector, Geant4 simulations of the response matrix, and verification of the spectrum unfolding results, etc.) was studied. Finally, the measured neutron pulse height spectra were successfully converted into neutron energy spectra, and the time evolution of the neutron energy spectrum obtained was analyzed.

The best time resolution of the neutron energy spectrum obtained is 100 ms. This time resolution means that the HL-3 tokamak has, for the first time, the ability to experimentally study the time evolution of the fast ion velocity distribution.

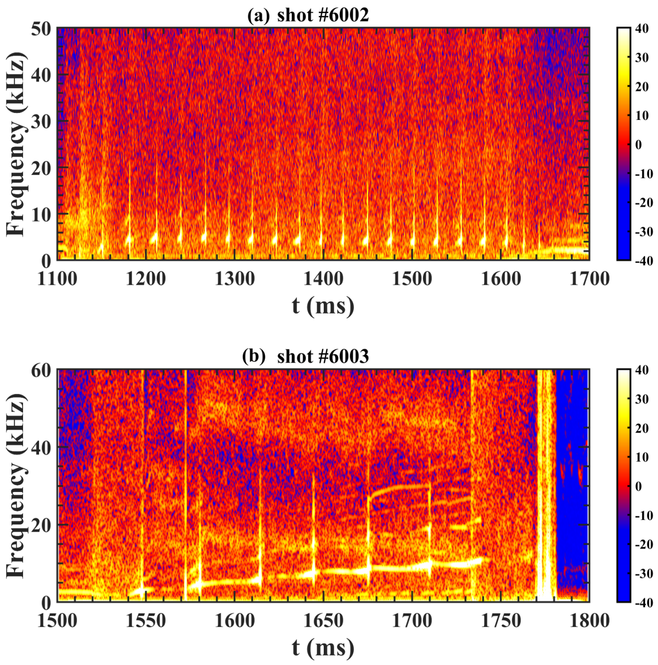

Fig. 13. (Color online) Frequency spectra of magnetic probe signals for shots (a) #6002 and (b) #6003. The MHD activity in shot #6002 is dominated by a sawtooth instability at approximately 40 Hz, whereas shot #6003 exhibits a dominant 1/1 mode whose frequency increases over time.

[1] S.D. Pinches, H.L. Berk, D.N. Borba et al., The role of energetic particles in fusion plasmas. Plasma Phys. Control. Fusion **46**, B187 (2004). doi: 10.1088/0741-3335/46/12B/017

[2] M. García-Muñoz, H.U. Fahrbach, S. Günter et al., Fast-ion losses due to high-frequency MHD perturbations in the ASDEX upgrade tokamak. Phys. Rev. Lett. **100**, 055005 (2008). doi:10.1103/PhysRevLett.100.055005

[3] D.S. Darrow, S.J. Zweben, Z. Chang et al., Observations of neutral beam and ICRF tail ion losses due to Alfven modes in TFTR. Nucl. Fusion **37**, 939 (1997). doi: 10.1088/0029-5515/37/7/I03

[4] M. Isobe, K. Toi, H. Matsushita et al., Studies of fast-ion transport induced by energetic particle modes using fast-particle diagnostics with high time resolution in CHS. Nucl. Fusion **46**, S918 (2006). doi: 10.1088/0029-5515/46/10/S08

[5] J. Zhang, Y. Zhang, W. Chen et al., Investigation of energetic ion losses induced by long-lived saturated internal mode with energetic particle diagnostics in the HL-2A tokamak. Nucl. Fusion **63**, 086014 (2023). doi: 10.1088/1741-4326/acdca5

[6] W.W. Heidbrink, J.G.Sadler, The behaviour of fast ions in tokamak experiments. Nucl. Fusion **34**, 535 (1994). doi: 10.1088/1674-1137/37/2/024102

[7] A.S. Jacobsen, M. Salewski, J. Eriksson et al., Velocity-space sensitivity of neutron spectrometry measurements. Nucl. Fusion **55**, 053013 (2015). doi: 10.1088/0029-5515/55/5/053013

[8] M.G. Johnson, L. Giacomelli, A. Hjalmarsson et al., The 2.5-MeV neutron time-of-flight spectrometer TOFOR for experiments at JET. Nucl. Instrum. Methods Phys. Res. A **591**, 417 (2008). doi: 10.1016/j.nima.2008.03.010

[9] A. Hjalmarsson, S. Conroy, G. Ericsson et al., The TOFOR spectrometer for 2.5 MeV neutron measurements at JET. Rev. Sci. Instrum. **74**, 1750 (2003). doi: 10.1063/1.1534401

[10] Y. Zhang, L. Ge, Z. Hu et al., The First Experimental Results of Time-of-Flight Neutron Spectrometer at EAST. J. Fusion Energ. **40**, 14 (2021). doi: 10.1007/s10894-021-00304-6

[11] M. Angelone, D. Lattanzi, M. Pillon et al., Development of single crystal diamond neutron detectors and test at JET tokamak. Nucl. Instrum. Methods Phys. Res. A **595**, 616–622 (2008). doi: 10.1016/j.nima.2008.07.107

[12] S.Y. Lin, R.J. Zhou, K.K. Artemev et al., Development of diamond detector as fast neutron spectroscopy in the EAST tokamak. J. Instrum. **19**, P07017 (2024). doi: 10.1088/1748-0221/19/07/P07017

[13] S. Sangaroon, K. Ogawa, M. Isobe, Neutron emission spectrometer in magnetic confinement fusion. AAPPS Bull. **34**, 34 (2024). doi: 10.1007/s43673-024-00139-1

[14] L.J. Ge, Z.M. Hu, Y.M. Zhang et al., Neutron emission spectroscopy measurements with a compact liquid scintillation detector for NBI-heated plasma at EAST. Plasma Phys. Control. Fusion **60**, 095004 (2018). doi: 10.1088/1361-6587/aad06c

[15] X. Xie, Z. Chen, X. Peng et al., Neutron emission measurement at the HL-2A tokamak device with a liquid scintillation detector. Rev. Sci. Instrum. **85**, 103506 (2014). doi: 10.1063/1.4896120

[16] X.R. Duan, M. Xu, W.L. Zhong et al., Recent advance progress of HL-3 experiments. Nucl. Fusion **64**, 112021 (2024). doi: 10.1088/1741-4326/ad6e9e

[17] H.Y. Shen, J.L. Zhang, J. Zhang et al., FPGA implementation

of 500-MHz high-count-rate high-time-resolution real-time digital neutron-gamma discrimination for fast liquid detectors. Nucl. Sci. Tech. **35**, 136 (2024). doi: 10.1007/s41365-024-01441-1

[18] X. Song, X.M. Song, B. Li et al., Plasma initiation and preliminary magnetic control in the HL-2M tokamak. Nucl. Fusion **61**, 086010 (2021). doi: 10.1088/1741-4326/ac09fc

[19] L. Xue, X.R. Duan, G.Y. Zheng et al., Effects of the second X-point on hot VDE in HL-2M. Nucl. Fusion **57**, 056029 (2017). DOI: 10.1088/1741-4326/aa65ab

[20] H. Liu, J. Cao, H. Wei et al., The latest progress of the 1st NBI beamline on HL–2M Tokamak. Fusion Eng. Des. **123**, 448–452 (2017). doi: 10.1016/j.fusengdes.2017.02.109

[21] M. Nocente, Fast-ion measurements with neutron and gamma-ray spectroscopy in thermonuclear plasmas: recent results and future prospects. IL Nuovo Cimento C **39**, 289 (2016). doi: 10.1393/ncc/i2016-16289-6

[22] J. Zhang,Y. Zhang, J. Yang et al., Influences of fusion neutrons on Compton suppressed γ-spectrum analyses at the HL-2A tokamak. Appl. Radiat. Isot. **166**, 109387 (2020). doi: 10.1016/j.apradiso.2020.109387

[23] J. Zhang, Y. Zhang, J. Zhang et al., Development of a high-temporal resolution neutron flux measurement system for the HL-2M tokamak. J. Instrum. **17**, P07027 (2022). doi: 10.1088/1748-0221/17/07/P07027

[24] G. Yuan, Z. Wen, L. Wei et al., Neutron yield measurement system of HL-2A tokamak. Plasma Sci. Technol. **24**, 064006 (2022). doi: 10.1088/2058-6272/ac4f40

[25] Y.P. Zhang, M. Isobe, Y. Liu et al., Measurements of the fast ion slowing-down times in the HL-2A tokamak and comparison to classical theory. Phys. Plasmas **19**, 112504 (2012). doi: 10.1063/1.4768425

[26] B. Wan, X.Y. Zhang, L. Chen et al., Digital pulse shape discrimination methods for n-γ separation in an EJ-301 liquid scintillation detector. Chinese Phys. C **39**, 116201 (2015). doi: 10.1088/1674-1137/39/11/116201

[27] M. Matzke, Unfolding of particle spectra. Proc. SPIE. **59**, 2867 (1997). doi: 10.1117/12.267860

[28] Y. Chen, X. Chen, J. Lei et al., Unfolding the fast neutron spectra of a BC501A liquid scintillation detector using GRAVEL method. Sci. China Phys. Mech. Astron. **57**, 1885–1890 (2014). doi: 10.1007/s11433-014-5553-7

[29] P.J. Green, On use of the EM algorithm for penalized likelihood estimation. J. R. Statist. Soc. B **52**, 443–452 (1990). doi: 10.1111/j.2517-6161.1990.tb01798.x

[30] A.V. Hristova, E.I. Vapirev, L.T. Tsankov et al., Compton edge energy calibration of organic detectors. Appl. Radiat. Isot. **41**, 887–889 (1990). doi: 10.1016/0883-2889(90)90068-R

[31] G.C. Chikkur, N. Umakantha, A new method of determining the compton edge in liquid scintillators. Nucl. Instrum. Methods Phys. Res. **107**, 201–202 (1973). doi: 10.1016/0029-554X(73)90034-7

[32] A. Sood, R.P. Gardner, A new Monte Carlo assisted approach to detector response functions. Nucl. Instrum. Methods Phys. Res. B **213**, 100–104 (2004). doi: 10.1016/S0168-583X(03)01540-4

[33] C.M. Salgado, L.E.B. Brandão, R. Schirru et al., Validation of a NaI(Tl) detector's model developed with MCNP-X code. Prog. Nucl. Energ. **59**, 19–25 (2012). doi: 10.1016/j.pnucene.2012.03.006

[34] C. Kim, Y. Kim,M. Moon et al., Iterative Monte Carlo simulation with the Compton kinematics-based GEB in a plastic scintillation detector. Nucl. Instrum. Methods Phys. Res. A **795**, 298–304 (2015). doi: 10.1016/j.nima.2015.06.007

[35] J. Allison, K. Amako, J. Apostolakis et al., Geant4 developments and applications. IEEE Trans. Nucl. Sci. **53**, 270–278 (2006). doi: 10.1109/TNS.2006.869826

[36] F. Pino, L. Stevanato, D. Cester et al., The light output and the detection efficiency of the liquid scintillator EJ-309. Appl. Radiat. Isot. **89**, 79–84 (2014). doi: 10.1016/j.apradiso.2014.02.016

[37] X.L. Chen, X. Qin, J. Liu et al., Design of an Am–Be neutron source experimental platform at Sichuan University. Appl. Radiat. Isot. **167**, 109443 (2021) doi: 10.1016/j.apradiso.2020.109443

[38] S.K. Cheng, Y.P. Zhang, Y.J. Shi et al., Geant4 simulation of fast-electron bremsstrahlung imaging at the HL-3 tokamak. Nucl. Sci. Tech. **35**, 159 (2024). doi: 10.1007/s41365-024-01505-2

[39] L.Y. Liao, K. Ogawa, M. Isobe et al., The multi-sightline compact D-D neutron spectrometers based on CLYC7-scintillator for beam ion anisotropy study in LHD. J. Instrum. **19**, P03006 (2024). doi: 10.1088/1748-0221/19/03/P03006

[40] G.L. Yuan, Simplified neutron peak width formula for thermonuclear fusion reactions. IEEE Trans. Plasma Sci. **50**, 1113–1114 (2022). doi: 10.1109/TPS.2022.3155153